Unaligned but Safe - Formally Compensating Performance Limitations for Imprecise 2D Object Detection[*]

Tobias Schuster*, Emmanouil Seferis*, Simon Burton, and Chih-Hong Cheng

Fraunhofer Institute for Cognitive Systems
Hansastr. 32, 80686 Munich, Germany

`{firstname.lastname}@iks.fraunhofer.de`

Abstract. In this paper, we consider the imperfection within machine learning-based 2D object detection and its impact on safety. We address a special sub-type of performance limitations: the prediction bounding box cannot be perfectly aligned with the ground truth, but the computed Intersection-over-Union metric is always larger than a given threshold. Under such type of performance limitation, we formally prove the minimum required bounding box enlargement factor to cover the ground truth. We then demonstrate that the factor can be mathematically adjusted to a smaller value, provided that the motion planner takes a fixed-length buffer in making its decisions. Finally, observing the difference between an empirically measured enlargement factor and our formally derived worst-case enlargement factor offers an interesting connection between the quantitative evidence (demonstrated by statistics) and the qualitative evidence (demonstrated by worst-case analysis).

Keywords: Safety · Object detection · Deep learning · Post-processing

1 Introduction

The safety of autonomous driving (AD) has become a crucial factor for industry in the admittance of AD functions. For realizing AD functions, deep neural networks (DNNs) are widely used to implement modules such as object detection. It is thus essential to systematically analyze the impact of performance limitations of DNNs; the purpose is to ensure that the limitations are properly compensated by system design and do not lead to unreasonable risks.

In this paper, we consider a special type of performance limitations, namely *bounding box non-alignment* in the 2D object detection setup. Bounding box non-alignment refers to the situation where the prediction can not suitably cover the object. It may impose safety risks, as any object not surrounded by the prediction

---

bounding box can be viewed as an empty space, thereby inducing the risk of collision. Such type of performance insufficiency is commonly characterized in training by computing the Intersection-over-Union (IoU) ratio between the ground-truth (GT) label bounding box and the prediction bounding box. Provided that the degree of insufficiency is bounded, which can characterized by the computed IoU ratio always being larger than a constant α, the key contribution of this paper is to formally derive the *minimum required enlargement factor* to be imposed on the prediction bounding box to fully cover the GT label. As a consequence, by adding a conservative post-processor after the DNN to enlarge the prediction bounding box using the derived enlargement factor, the imprecision (to the degree governed by α) is guaranteed not to have a safety impact.

Subsequently, we consider the allocation problem for the computed bounding box enlargement. Following the practical observation that the motion planner always reserves a fixed width as a safe buffer, one can thus utilize the buffer and employ a smaller enlargement, provided that the combined effect of the bounding box enlargement (from the safety post-processor) and the buffer from the motion planner is larger than the computed bound. We show that such a sound estimation that guarantees safety is conditional to an assumption over the maximum width of the detected object type (e.g., car).

Finally, we compare the formally derived enlargement factor with an enlargement factor directly *measured from the training data*, following the methodology in [4]. There can be many interpretations over the value gap. Obviously, the measured enlargement factor to cover the GT label bounding box is smaller, as the formal derivation considers *the worst case scenario* while the worst case scenario may not be present in the training dataset. However, considering the distance between the measured mean enlargement factor to the worst-case computed factor also offers an interesting link between the quantitative evidence (as supported by statistics) and the qualitative evidence (as supported by the worst-case analysis), as gap can be further rewritten by the multiple of the standard deviation σ measured from data.

The rest of the paper is structured as follows. After reviewing related work in Section 2, in Section 3 we summarize the basic principles of the conservative post-processing algorithm. In Section 4 we derive the connection between IoU and safety and subsequently in Section 5, we consider the situation where motion planners also reserve some buffer to compensate the imprecision. Finally, we evaluate the result by comparing the formal result with the data-driven approach using a case study in Section 6, and conclude in Section 7 by outlining further research opportunities.

2   Related Work

The safety of DNNs is currently researched from different angles; we recommend readers to a current survey [5] conducted by the German national project KI-Absicherung for an overview. On the methodology side, many results on safety argumentation use semi-formal/structural notations with variations on
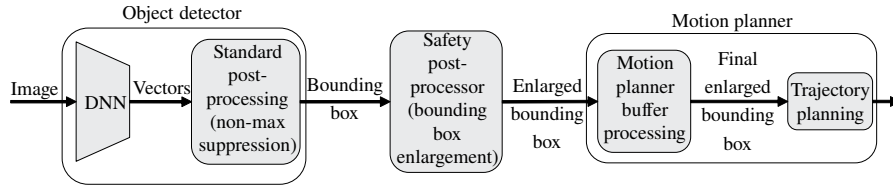
argumentation strategies (to list a few [2,17,8,14]). The value of these results is the offering of a generic argumentation structure, where the purpose of this paper is to demonstrate its implementation aspects for one type of performance insufficiencies. For DNN testing, apart from proposing concrete testing techniques [13], another key direction is to introduce new coverage criteria where the goal is to include diversified test cases such that the computed coverage is sufficiently high. For the white box coverage criteria, neuron coverage [12] and extensions (e.g., SS-coverage [15]) motivated by MC/DC coverage in classical software have been proposed. For the black box coverage criteria, multiple results are utilizing combinatorial testing [3,1] to argue about the relative completeness of the test data. Readers may reference Section 5.1 of a recent survey paper [6] for an overview of existing results in coverage-driven testing. However, the key issue for these coverage criteria is that they do not have a direct connection to safety, which is in many cases task specific. Very recently, Lyssenko et al. [11] proposed to include a task-oriented relevance factor in the evaluation of DNNs. They used the distance from the sensor to object to derive a relevance metric based on the IoU with a focus on semantic segmentation. Additionally, Volk et al. [16] defined a comprehensive safety score by considering various factors such as quality, relevance, and reaction time. The safety score is based on extending the basic IoU value. Again, to be used in safety argumentation, these metrics need to be connected to concrete performance limitations and to concrete applications, as suggested in safety standards such as ISO 21448 [7]. Our result overcomes the above mentioned limitation: even for the commonly used IoU metric, we can establish a precise and mathematically sound connection with the safety goal by properly restricting ourselves to a particular performance limitation of non-aligning bounding boxes.

Finally, the recent work from Cheng et al. [4] initiated the concept of safety post-processing attached to the standard post-processor to address the insufficiency of imprecise prediction. In [4], one estimates the enlargement threshold based on the data. This is in contrast to the concept stated in this paper where the enlargement factor is computed using worst-case analysis. The safety guarantee of the data-driven approach is conditional to an assumption on the generalizability between in-sample and out-of-sample data; this is not the case for our worst-case derivation. The data-driven and the logical approach complement each other; in our experiments we also consider their connection.

3   Data-driven Safe Post-Processing in Addressing 2D Object Detection Imprecision

We first review the commonly used definition of the IoU between two rectangles.

Definition 1. *Given two 2D rectangles R_A and R_B, the intersection-over-union is defined to be the ratio between the overlapping area of R_A and R_B (nominator) and the union area of R_A and R_B (denominator), where $\mathsf{area}(R)$ devotes the area*

Fig. 1. The safety post-processor is inserted between the object detector and the motion planer. Here sensor fusion is omitted for simplicity purposes; the basic principle still applies when sensor fusion modules are introduced.
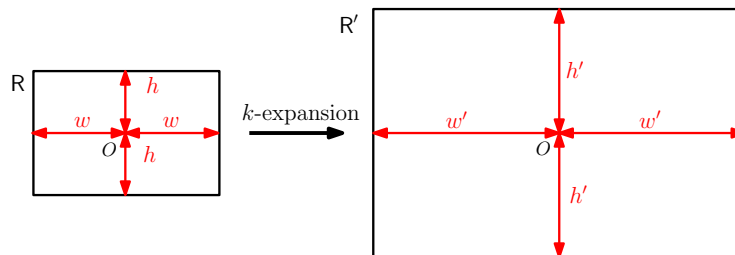
of some region R on the 2D plane.

$$IoU(R_A, R_B) = \frac{area(R_A \cap R_B)}{area(R_A \cup R_B)} \tag{1}$$

Within 2D object detection, the two rectangles used for calculating the IoU are the prediction bounding box R_{PR} and the associated GT bounding box R_{GT}. We also assume that all considered bounding boxes are horizontally laid out rectangles, i.e., all rectangles are *axis-aligned*.

We now summarize the principle of safe post-processors (SPP) as defined in [4] using Figure 1, where introducing the post-processor between object detector and motion planner is meant to *compensate the performance insufficiency caused by non-alignment between prediction bounding box and GT label bounding box*. While the general principle is applicable also for 3D detection, in this paper we restrict ourselves to the discussion on 2D front-view detection.

1. For each image collected in the training dataset, and for each predicted bounding box (R_{PR_i}) that only partially covers the associated GT bounding box R_{GT_i} but has $IoU(R_{PR_i}, R_{GT_i}) \geq \alpha$, one measures the minimum enlargement factor required to enclose the GT bounding box. An illustration is shown in Figure 3, where as R_{PR} does not enclose R_{GT}: one can properly enlarge R_{PR} to $R_{PR'}$, and the enlargement factor from R_{PR} to $R_{PR'}$ is the ratio of two widths (or two heights) between the two rectangles.
2. Aggregate the enlargement factor for all images in the training dataset and for all bounding boxes analyzed in the previous step. This can be done by taking the maximum value, further denoted as $k_{max,data}$, or by taking the mean value $k_{\mu,data}$ plus some additional buffers if desired.
3. Finally, add an SPP unit after the standard bounding box detector, as illustrated in Figure 1. During operation, for each image captured by a camera sensor, the SPP always enlarges each predicted bounding box by the factor computed in the previous step.

This method for determining the enlargement factor is *learned/measured from the training data*, where in the following section, we will describe a method that computes the required enlargement factor by conservatively considering, under the condition where $IoU(R_{PR}, R_{GT}) \geq \alpha$, all possible overlapping scenarios.

Fig. 2. A rectangle R (left), and it's k-expansion R′ (right)

4 Mathematically Associating the IoU Metric and Safety

In this section, we present the key result of the paper, namely the formal derivation of the *minimum required enlargement factor* to fully cover the ground truth bounding box (a situation that we refer to be "safe"), under the condition $\mathsf{IoU} \geq \alpha$, by considering *the theoretical worst case scenario.*

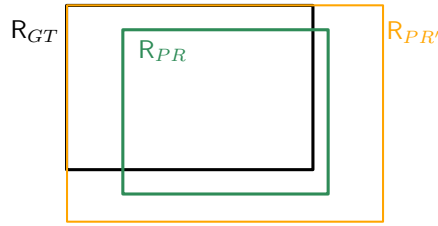### 4.1 The Mathematical Connection between IoU and Safety

We first formally define the enlargement factor with the help of Figure 2. Consider a rectangle R with center O, half-width w and half-height h, as depicted on the left of Figure 2. Then the definition of an enlargement factor can be stated using Definition 2. The enlarged rectangle R′ is shown on the right of Figure 2. Note that this is equivalent to multiplying the length and width of R by k, while keeping the center fixed.

Definition 2. *The k-expansion ($k \geq 1$) transforms a rectangle R to a new rectangle R′ by keeping the center O fixed while multiplying w, h by k, i.e., $w' = k \cdot w$, $h' = k \cdot h$. The value k is called the enlargement factor.*
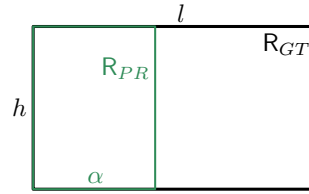
Assuming that no safety-aware post-processing exists, a complete enclosure of an object (in training or testing, an object is represented by the GT label) by the predicted bounding box is necessary to achieve safe detection. However, when considering a safety-aware post-processing step that enlarges the predicted bounding box by a certain margin, the risk due to a small amount of imprecision in detection can be compensated by the enlargement strategy. As a consequence, the IoU metric could still be used to determine a safe detection and leads to the following research question:

Question 1. Within 2D object detection, assume that a ground-truth label R_{GT} is intersecting with the prediction R_{PR}, both as horizontally laid out rectangles as shown in Figure 3, with an $\mathsf{IoU}(\mathsf{R}_{GT}, \mathsf{R}_{PR}) \geq \alpha$, where $\alpha \in (0, 1]$. What is the minimum k-expansion to be applied on R_{PR} such that it can fully cover R_{GT}?

We introduce the following example as a special case, which is later used in answering Question 1.

Fig. 3. The ground-truth labeling bounding box R_{GT}, prediction R_{PR}, and the k-expanded prediction $\mathsf{R}_{PR'}$ that covers R_{GT}.

Fig. 4. A special case where R_{GT} and R_{PR} have the same height.

Example 1. Consider the ground-truth label R_{GT}, and the prediction R_{PR} that is fully covered by R_{GT} and only deviating from R_{GT} in one direction as depicted in Figure 4. Let the width of R_{GT} to be l and the height to be h and let the prediction width be αl. What is the minimum k-expansion so that the k-expanded R_{PR} covers R_{GT}?

(Solution to Example 1) Note that the height dimension is already covered, therefore, we focus on the width. Currently, the half-width of PR is $w = \frac{\alpha l}{2}$. In order to cover R_{GT}, the half-width w of R_{PR} has to increase by the distance $l - \alpha l$, to reach the bottom-right corner of R_{GT} to cover it. Thus, the new half-width will be $w' = w + (l - \alpha l)$, and the minimum k value is:

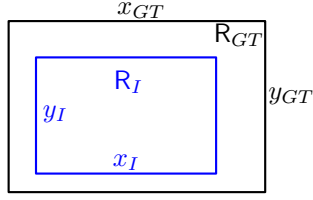$$k = \frac{w'}{w} = \frac{\frac{\alpha l}{2} + l - \alpha l}{\frac{\alpha l}{2}} = \frac{2 - \alpha}{\alpha}$$

Moreover, noticing that the IoU in this case is exactly α, we can also express k in terms of the IoU:

$$k = \frac{2 - \mathsf{IoU}(\mathsf{R}_{PR}, \mathsf{R}_{GT})}{\mathsf{IoU}(\mathsf{R}_{PR}, \mathsf{R}_{GT})} \tag{2}$$
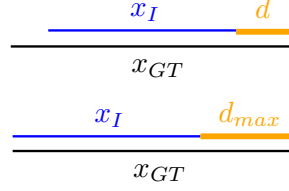
$\square$

Before extending the previous example to the general case of Question 1, we introduce the following required Lemma 1, which states that an axis-aligned rectangle contained in a larger axis-aligned rectangle will still be contained when enlarging both rectangles with the same factor $k \geq 1$. This is based on the fact that the expansion does not change the center for R' and R. Therefore, when both rectangles enlarge themselves by an identical constant factor, the original area containment relation remains. The complete proof can be found in Appendix A.1.

Lemma 1. *Consider an axis-aligned rectangle R, and a second axis-aligned rectangle R' that contains R. The region containment relation holds subject to the k-expansion, i.e., the k-expanded R will still be contained in the k-expanded R', for any $k \geq 1$.*

Fig. 5. Example ground-truth (black) and intersection (blue) rectangle.

Fig. 6. The two line segments x_{GT}, x_I and the distance d between them.

We now state the main theorem and its proof answering Question 1, where it turns out that the situation stated in Example 1 actually characterizes *the theoretical worst case scenario* between the prediction bounding box and GT label.

Theorem 1. *Let $\alpha \in (0,1]$ be a constant, and let R_{PR} and R_{GT} be the axis-aligned prediction and ground-truth bounding boxes that satisfy the following constraint:*

$$\mathsf{IoU}(R_{PR}, R_{GT}) \geq \alpha$$

Then the minimum k-expansion for R_{PR} to cover R_{GT} is characterized by $k = \frac{2-\alpha}{\alpha}$.

Proof. There are many different cases for the intersection and union between the prediction and GT rectangles (e.g., prediction overlapping with GT, prediction completely inside GT, etc.). Therefore, we start the proof by considering the relation between the GT label and the *intersection*, not the prediction. This leads to a simplified sub-problem where we can solve easily and find the required k value. Subsequently, by using Lemma 1, we extrapolate from the intersection to the prediction bounding box and finally, we show the tightness of the result.

We denote the intersection of R_{GT} and R_{PR} as R_I, and their union by R_U. Moreover, we denote the areas of R_{GT}, R_I and R_U as $\mathsf{area}(\mathsf{R}_{GT})$, $\mathsf{area}(\mathsf{R}_I)$ and $\mathsf{area}(\mathsf{R}_U)$. From Definition 1 of the IoU, we derive:

$$\mathsf{IoU}(\mathsf{R}_{GT}, \mathsf{R}_{PR}) = \frac{\mathsf{area}(\mathsf{R}_I)}{\mathsf{area}(\mathsf{R}_U)} \geq \alpha \tag{3}$$

Since the $\mathsf{area}(\mathsf{R}_U)$ is always larger or equal to $\mathsf{area}(\mathsf{R}_{GT})$, we derive:

$$\alpha \leq \mathsf{IoU}(\mathsf{R}_{GT}, \mathsf{R}_{PR}) = \frac{\mathsf{area}(\mathsf{R}_I)}{\mathsf{area}(\mathsf{R}_U)} \leq \frac{\mathsf{area}(\mathsf{R}_I)}{\mathsf{area}(\mathsf{R}_{GT})} \Leftrightarrow \mathsf{area}(\mathsf{R}_{GT}) \leq \frac{\mathsf{area}(\mathsf{R}_I)}{\alpha} \tag{4}$$

Consider now the intersection and the GT label as shown in Figure 5. Note that Figure 5 represents only one case; in fact, the only prerequisite for the proof is that the intersection is contained in R_{GT} - its exact location does not change the proof. Let x_{GT} and y_{GT} be the width and height of R_{GT}, and let x_I and y_I be the width and height of the intersection R_I respectively in Figure 5. Let $r_x = x_{GT}/x_I$ be the ratio of the widths of R_{GT} and R_I, and $r_y = y_{GT}/y_I$ the

ratio of the heights of R_{GT} and R_I. Then, the area of R_{GT} in terms of r_x, r_y is given by Equation 5.

$$\mathsf{area}(\mathsf{R}_{GT}) = x_{GT} \cdot y_{GT} = r_x x_I \cdot r_y y_I = r_x r_y (x_I \cdot y_I) = r_x r_y \mathsf{area}(\mathsf{R}_I) \quad (5)$$

From Equation 4 it is known that $\mathsf{area}(\mathsf{R}_{GT}) \leq \mathsf{area}(\mathsf{R}_I)/\alpha$, thus, combining it with Equation 5, we get Equation 6.

$$\mathsf{area}(\mathsf{R}_{GT}) = r_x r_y \mathsf{area}(\mathsf{R}_I) \leq \frac{\mathsf{area}(\mathsf{R}_I)}{\alpha} \Leftrightarrow r_x r_y \leq \frac{1}{\alpha} \quad (6)$$

That is, the product of r_x, r_y is bounded by $\frac{1}{\alpha}$. Since $r_x \geq 1, r_y \geq 1$ (the intersection is contained in GT and cannot be larger than GT), the maximum value one can take for one of these ratios is $\frac{1}{\alpha}$. Without loss of generality, we consider the width (the proof can be derived for the height in the same way). That is, x_{GT} is at most $\frac{x_I}{\alpha}$ due to the below inequality:

$$x_{GT} = r_x x_I \leq \frac{1}{\alpha} \cdot x_I = \frac{x_I}{\alpha} \quad (7)$$

Given that, how much do we need to k-expand x_I in order to cover x_{GT}? Now, we can focus solely on the line segments x_{GT} and x_I, as shown in Figure 6. For x_I to cover x_{GT}, we must add the distance d from the endpoint of x_I up to the endpoint of x_{GT}. This distance is at most $d \leq d_{max} = x_{GT} - x_I$, since x_I is contained within x_{GT}, and occurs when x_I and x_{GT} align on one side. Therefore, the original half-width $w_I = \frac{x_I}{2}$ of the intersection must increase at most by a distance $d_{max} = x_{GT} - x_I$, leading to (using Equation 7) the following enlarged half-width in the worst case (maximum possible):

$$w_I' \leq w_I + d_{max} = w_I + x_{GT} - x_I \leq w_I + x_I(\frac{1}{\alpha} - 1) \Rightarrow$$
$$w_{I,max}' = w_I + x_I(\frac{1}{\alpha} - 1) \quad (8)$$

With this, the worst-case expansion factor k for R_I to cover R_{GT} will be

$$k = \frac{w_{I,max}'}{w_I} = \frac{w_I + x_I(\frac{1}{\alpha} - 1)}{w_I} \Rightarrow$$
$$k = \frac{\frac{x_I}{2} + x_I(\frac{1}{\alpha} - 1)}{\frac{x_I}{2}} \Leftrightarrow$$
$$k = \frac{x_I + 2x_I(\frac{1}{\alpha} - 1)}{x_I} \Leftrightarrow \quad (9)$$
$$k = 1 + 2(\frac{1}{\alpha} - 1) = \frac{2}{\alpha} - 1 \Leftrightarrow$$
$$k = \frac{2 - \alpha}{\alpha}$$

Now, the rectangle that should be expanded is the prediction R_{PR}, not the intersection R_I. However, due to Lemma 1, since R_{PR} contains the intersection R_I, the k-expanded R_{PR} will contain the k-expanded intersection, which in turn contains R_{GT}. Thus, expanding R_{PR} by k can also cover R_{GT} in all cases.
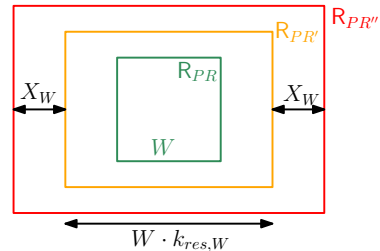
Finally, the bound k obtained in Equation 9 for expanding R_{PR} is tight, since there are cases such as Example 1 where $k = \frac{2-\alpha}{\alpha}$ is necessary. This concludes the proof.

<div align="right">□</div>

The consequence of Theorem 1 is that by inverting Question 1, one can compute a safe IoU threshold based on a fixed k value[1]. From now on, the *theoretically derived* k value using Theorem 1 will be denoted as k_{math}.

5 Connecting Motion Planners with Safety Post-Processing

In this section, we present the mathematical relation between motion planning and safety-aware post-processing. As can be seen in Figure 1, after the prediction bounding boxes are enlarged by the SPP, the enlarged predictions are then passed to the motion planner that can also add a physical buffer before planning the trajectory. However, the formally derived k value in Section 4.1 assumes no extra motion planner buffer to be applied to the enlarged bounding box. If the motion planner always adds a physical buffer to the enlarged bounding box, it is not

Fig. 7. Motion planner buffer enlargement on top of safety post-processing. R_{PR} denotes the predicted bounding box, $\mathsf{R}_{PR'}$ the k-expanded R_{PR} and $\mathsf{R}_{PR''}$ the $\mathsf{R}_{PR'}$ with additional motion planner buffer X_W.

required to apply the SPP with a k value following Theorem 1. More precisely, as long as the effect of the SPP and the motion planner is larger than the k value from Theorem 1, the prediction can be considered safe.

Precisely, let $k_{res,W}$ be the (residual) enlargement factor for the width (similar methodology equally applicable to height) when considering the physical buffer X_W to be added by the motion planner to each bounding box on both sides, as seen in Figure 7. Furthermore, we consider that a prediction bounding box R_{PR} of an object has an initial physical width of W. After applying $k_{res,W}$, the new width is $W \cdot k_{res,W}$. Finally, considering the motion planner buffer, the final width is $2X_W + Wk_{res,W}$. Then, the effect of SPP and motion planner can be characterized by Equation 10, which requires that the total enlargement factor due to the SPP and the motion planner exceeds the given enlargement threshold k_{math} derived from Theorem 1. For simplicity, in this paper we further

---

[1] Due to space limits, we refer readers to Appendix A.3 for further details.

assume that all objects as well as the point-of-view are placed on a flat surface environment.

$$\frac{\frac{2X_W + Wk_{res,W}}{2}}{\frac{W}{2}} \geq k_{math} \Leftrightarrow$$
$$\frac{2X_W}{W} + k_{res,W} \geq k_{math} \tag{10}$$

Further, by transforming Equation 10 we derive the $k_{res,W}$ value to be used by the SPP in Equation 11. As one can see, the smallest $k_{res,W}$ guaranteeing safety is determined by the lower bound of combined enlargement k as well as the physical motion planner buffer X_W, and is conditional on an assumption over the **maximum observed width** W_{max} of the detected object type, e.g, "car". Furthermore, note that the SPP does not decrease the bounding box size, leading to the constraint in Equation 12. Combining Equation 11 and 12 leads to the minimum $k_{res,W}$ value $k_{res,W,min}$ determined by Equation 13.

$$k_{res,W} \geq k_{math} - \frac{2X_W}{W} \tag{11}$$

$$k_{res,W} \geq 1 \tag{12}$$

$$k_{res,W,min} = max\left(k_{math} - \frac{2X_W}{W_{max}}, 1\right) \tag{13}$$

Situations when W_{max} appears can be computed analytically. Consider the identified object to be of class "car". One can derive that the largest observed width occurs when a "car" object satisfies the following two conditions:

- The car's diagonal has maximum length.
- The car's diagonal is oriented 90° towards the ego vehicle's front-facing axis.

As an example, let the physical buffer be $X_W = 50cm$ and $k_{math}(\alpha = 0.5) = 3$. According to German traffic law, the largest "car" has a width of $250cm$ and a length of $700cm$. Therefore, the largest observed object width will be the diagonal, i.e., $W_{max,car} = \sqrt{700^2 + 250^2} = 743cm$. These considerations result in the enlargement factor $k_{res,W,min,car} = 2.87$ for the object with type "car". For any other "car" object with an observed width $W'_{car} \leq W_{max,car}$, the combined enlargement is larger or equal to k_{math}.

$$\frac{2X_W}{W'_{car}} + k_{res,W,min,car} \geq \frac{2X_W}{W_{max,car}} + k_{res,W,min,car} = k_{math} \tag{14}$$

Here we omit further details, but a similar analysis technique can be applied for the height of the detected objects. Finally, the similar analysis technique is also applicable for data-driven SPP as stated in Section 3: instead of taking the formally derived k_{math} in Theorem 1, one simply replaces k_{math} by the measured value such as $k_{max,data}$.

6 Evaluation

We perform an empirical study to understand the difference between an empirically measured enlargement factor (cf Section 3) and our formally derived worst-case enlargement factor (using Theorem 1). This overall offers an interesting connection between the quantitative evidence (demonstrated by statistics) and qualitative evidence (demonstrated by worst-case analysis).

For the case study, we choose YOLO V5s [9], a single-stage object detector pretrained on the COCO dataset [10]. Moreover, we use a small automotive image dataset[2] generated with the CARLA[3] simulator, containing 820 training images and 208 test images with objects of the classes bike, motorbike, traffic light, traffic sign and vehicle which was split into car and truck. The dataset is generated via driving in autopilot, taking images from the ego vehicles perspective and the bounding box labels were generated from the semantic segmentation information with manual adjustment and correction afterwards. All other hyperparameters remain default (and are not tuned as we are not interested in finding the best model but rather want to show the connection between IoU and safety). For training and validation, we apply a 90-10 split, resulting in 738 and 82 images for the respective datasets. For generating the predictions on the training dataset, we set the standard post-processing parameters confidence threshold and non-maximum suppression threshold to be 0.5. Based on the above configuration, for a given IoU threshold value α from 0.1 to 0.9, we have conducted the following experiments for the width of the object class "car":

1. **Mathematical worst-case enlargement factor** First, we derive the mathematical worst-case k value k_{math} following Theorem 1 where no physical buffer is assigned. The results are reflected in the first row of Table 1.
2. **Data-enabled worst-case enlargement factor** We further use the method in Section 3 to derive the measured worst-case k value where no physical buffer is assigned. $k_{max,W,data}$ records the maximum observed enlargement factor for width in the second row of Table 1.
3. **Data-enabled average enlargement factor** We again use the method in Section 3 to derive the measured average k value $k_{\mu,W,data}$ and the standard deviation $\sigma_{W,data}$ for width where no physical buffer is assigned. They are recorded in Table 1, row three and four. Additionally, we record the measured average k value plus three standard deviations $(k_{\mu,W,data} + 3\sigma_{W,data})$ and plus six standard deviations $(k_{\mu,W,data} + 6\sigma_{W,data})$, with values stored in Table 1, row five and six.
4. **Combined effect of SPP and motion planner** Lastly, we investigate the combination of SPP and motion planner buffer by analyzing the influence of the physical buffer for width X_W on the $k_{res,W,min}$ values.
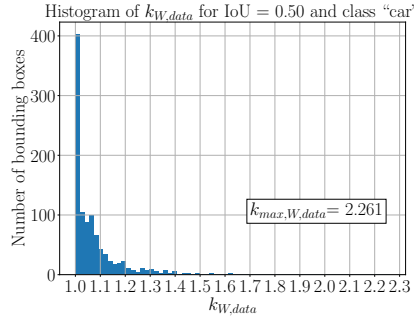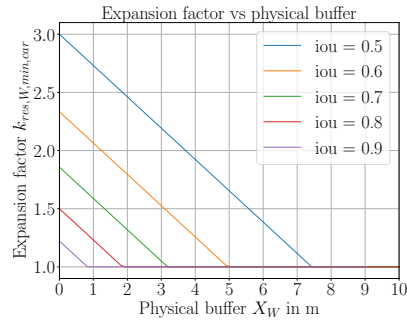
Mathematical and Measured Enlargement Factors We first compare the *measured* and *formally derived* k values by comparing the first and the second rows of Table 1.

Table 1. The formally derived and measured k values for the object class "car".

α	0.1	0.2	0.3	0.4	0.5	0.6	0.7	0.8	0.9
k_{math}	19.000	9.000	5.667	4.000	3.000	2.333	1.857	1.500	1.222
$k_{max,W,data}$	4.400	2.360	2.360	2.360	2.261	2.000	1.588	1.444	1.128
$k_{\mu,W,data}$	1.083	1.078	1.078	1.078	1.075	1.070	1.057	1.044	1.023
$\sigma_{W,data}$	0.176	0.130	0.130	0.129	0.118	0.105	0.078	0.058	0.030
$k_{\mu,W,data} + 3\sigma_{W,data}$	1.612	1.468	1.468	1.464	1.428	1.383	1.291	1.216	1.112
$k_{\mu,W,data} + 6\sigma_{W,data}$	2.141	1.857	1.857	1.850	1.780	1.697	1.524	1.389	1.202

Fig. 8. Histogram of $k_{W,data}$ values for class "car" at IoU ≥ 0.5.

Fig. 9. The relation between $k_{res,W,min}$ and X_W for class "car" with respect to varying IoU values.

Without surprise, we can observe that $k_{math} > k_{max,W,data}$, i.e., all k values observed on the data are lower than the theoretical ones. This is expected since the mathematically derived k-expansion factor provably considers all possible cases, but these worst cases rarely appear in reality. Moreover, one can observe that for an increasing IoU threshold, the measured values $k_{max,W,data}$ and $k_{\mu,W,data}$ decrease, similarly to the mathematical value k_{math}, as the predicted bounding boxes deviate less from the GT bounding box with increasing IoU. Additionally, we observe the following points:

1. For high IoU thresholds like 0.8 or 0.9, the measured worst case value $k_{max,W,data}$ and $k_{\mu,W,data} + 6\sigma_{W,data}$ are only slightly lower than the theoretical worst case value k_{math}. Considering low IoU values like 0.1 or 0.2, we observe the opposite; the measured worst case value $k_{max,W,data}$ and $k_{\mu,W,data} + 6\sigma_{W,data}$ are significantly lower than the theoretical worst case k_{math}.[4]
2. From the distribution of measured k values $k_{W,data}$, e.g. for IoU ≥ 0.5 in Figure 8, we can observe that it is a one-sided distribution with the majority of values close to one. Still, the probability of requiring a large k value is low.

---

[4] If we assume that the occurrence of bounding box non-alignment is a random variable, and the measured mean and variance match the real ones, then from the Chebyshev's inequality we know that the probability of exceeding $6\sigma_{W,data}$ is below 2.78%.

3. We see that for any IoU threshold, the distance between k_{math} and $k_{max,W,data}$ is always larger than three standard deviations $\sigma_{W,data}$, except for $\mathsf{IoU} \geq 0.8$.

Connecting SPP and Motion Planner We present the results of experiment 4 on the connection between the SPP and the motion planner buffer. For different thresholds IoU_{thres} and k_{math} values, assuming a maximum observed "car" width of $W_{max,car} = 7.43m$, we can derive $k_{res,W,min,car}$ as a function of the physical buffer X_W using Equation 13. The result is visualized by Figure 9, where we plot $k_{res,W,min,car}$ with respect to X_W for various IoU thresholds.

From Figure 9, we can observe that $k_{res,W,min,car} = 1$ when the physical buffer exceeds a certain value. Indeed, as we can also see from Equation 13, when the physical buffer becomes large enough and surpasses a threshold $X_{W,thres}$, the motion planner is by itself sufficient to guarantee safety, and no further enlargement by the SPP module is required. Otherwise, without a physical buffer, the enlargement is purely based on the SPP module. Moreover, we can see that this threshold value $X_{W,thres}$ is larger for lower IoU values. This is also reasonable, since for a small IoU, a larger physical buffer is necessary to guarantee safety. Finally, for large IoU values such as $\mathsf{IoU} \geq 0.9$, a physical buffer of $X_{W,thres} = 0.82m$ or larger can guarantee safety by itself.

7   Concluding Remarks

In this paper, we presented a formal approach to counteract the DNN performance insufficiency regarding *bounding box non-alignment*. The result is subject to the condition that the non-alignment is under control, i.e., characterized by the computed IoU being always larger than a fixed threshold. The main result of this paper (Theorem 1) provides a criterion to conservatively enlarge the prediction bounding box via an additional post-processing step after DNN-based object detection, in order to safely cover the object. We further studied the case when the motion planner also reserves some buffer, where the introduced post-processing and the buffer should altogether achieve the expansion governed by Theorem 1. Having such a unified analysis ensures that the resulting system is not acting overly conservatively without considering the capabilities of other components. Finally, our empirical evaluation on a simulation-based dataset demonstrates that the mathematically derived expansion factor is mostly larger than the empirically measured one with one standard deviation.

This work continues our vision of offering a rigorous methodology to systematically analyze performance limitations for DNNs and subsequently, provide counter-measures that are rooted in scientific rigor. We conclude by outlining some research directions currently under investigation: (a) Consider other types of DNN insufficiencies such as false negatives (disappearing objects) or false positives (ghost objects). (b) Extend the formalism by considering the interplay among multiple perception pipelines and the resulting sensor fusion. (c) Extend the theoretical framework to also cover DNN insufficiencies in 3D object detection. (d) Consider a fine-grained IoU metric and the corresponding worst-case expansion that is less conservative.
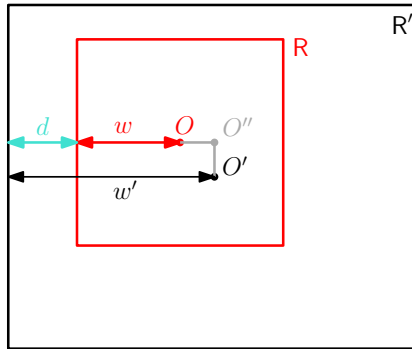
References

1. Abrecht, S., Gauerhof, L., Gladisch, C., Groh, K., Heinzemann, C., Woehrle, M.: Testing deep learning-based visual perception for automated driving. ACM TCPS **5**(4), 1–28 (2021)
2. Burton, S., Gauerhof, L., Heinzemann, C.: Making the case for safety of machine learning in highly automated driving. In: ASSURE. LNCS, vol. 10489, pp. 5–16. Springer (2017)
3. Cheng, C.H., Huang, C.H., Yasuoka, H.: Quantitative projection coverage for testing ML-enabled autonomous systems. In: ATVA. LNCS, vol. 11138, pp. 126–142. Springer (2018)
4. Cheng, C.H., Schuster, T., Burton, S.: Logically sound arguments for the effectiveness of ML safety measures. arXiv preprint arXiv:2111.02649 (2021)
5. Houben, S., Abrecht, S., Akila, M., Bär, A., Brockherde, F., Feifel, P., Fingscheidt, T., Gannamaneni, S.S., Ghobadi, S.E., Hammam, A., et al.: Inspect, understand, overcome: a survey of practical methods for ai safety. arXiv preprint arXiv:2104.14235 (2021)
6. Huang, X., Kroening, D., Ruan, W., Sharp, J., Sun, Y., Thamo, E., Wu, M., Yi, X.: A survey of safety and trustworthiness of deep neural networks: Verification, testing, adversarial attack and defence, and interpretability. Computer Science Review **37**, 100270 (2020)
7. Safety of the intended functionality - SOTIF (ISO/DIS 21448). Standard, International Organization for Standardization (2021)
8. Jia, Y., Lawton, T., McDermid, J., Rojas, E., Habli, I.: A framework for assurance of medication safety using machine learning. arXiv preprint arXiv:2101.05620 (2021)
9. Jocher, G., et al.: ultralytics/yolov5: v4.0 - nn.SiLU() activations, weights & biases logging, PyTorch hub integration, `https://zenodo.org/record/4418161`
10. Lin, T.Y., Maire, M., Belongie, S., Hays, J., Perona, P., Ramanan, D., Dollár, P., Zitnick, C.L.: Microsoft COCO: Common objects in context. In: ECCV. LNCS, vol. 8695, pp. 740–755. Springer (2014)
11. Lyssenko, M., Gladisch, C., Heinzemann, C., Woehrle, M., Triebel, R.: From evaluation to verification: Towards task-oriented relevance metrics for pedestrian detection in safety-critical domains. In: CVPR Workshop. pp. 38–45. IEEE (2021)
12. Pei, K., Cao, Y., Yang, J., Jana, S.: Deepxplore: Automated whitebox testing of deep learning systems. In: SOSP. pp. 1–18. ACM (2017)
13. Pezzementi, Z., Tabor, T., Yim, S., Chang, J.K., Drozd, B., Guttendorf, D., Wagner, M., Koopman, P.: Putting image manipulations in context: Robustness testing for safe perception. In: SSRR. pp. 1–8. IEEE (2018)
14. Salay, R., Czarnecki, K., Kuwajima, H., Yasuoka, H., Nakae, T., Abdelzad, V., Huang, C., Kahn, M., Nguyen, V.D.: The missing link: Developing a safety case for perception components in automated driving. arXiv preprint arXiv:2108.13294 (2021)
15. Sun, Y., Huang, X., Kroening, D., Sharp, J., Hill, M., Ashmore, R.: Structural test coverage criteria for deep neural networks. ACM TECS **18**(5s), 1–23 (2019)
16. Volk, G., Gamerdinger, J., Bernuth, A.v., Bringmann, O.: A comprehensive safety metric to evaluate perception in autonomous systems. In: ITSC. pp. 1–8. IEEE (2020)
17. Zhao, X., Banks, A., Sharp, J., Robu, V., Flynn, D., Fisher, M., Huang, X.: A safety framework for critical systems utilising deep neural networks. In: SAFECOMP. LNCS, vol. 12234, pp. 244–259. Springer (2020)

A   Appendix

A.1   Proof of Lemma 1

Lemma 1. *Consider an axis-aligned rectangle* R*, and a second axis-aligned rectangle* R′ *that contains* R*, as illustrated in Figure 10. The region containment relation* R $\subseteq$ R′ *holds subject to the k-expansion, i.e., the k-expanded* R *will still be contained in the k-expanded* R′*, for any* $k \geq 1$.

Fig. 10. The rectangle R′ containing a smaller rectangle R.

Proof. Let O be the center of R, O' the center of R′, and w, w' be the half-widths of R and R′ respectively. Consider, without loss of generality, the signed distance d from the left side of R to R′. Note from the figure that d will be equal to
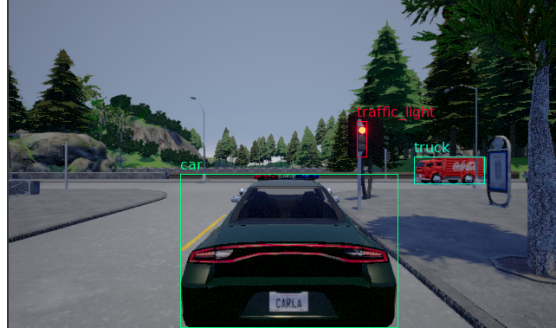
$$d = w' - w - |OO''|$$

where $|OO''|$ is the horizontal distance of the two centers, and is fixed. After the k-expansion of both rectangles, the new signed distance d_k will be

$$d_k = k \cdot w' - k \cdot w - |OO''| = k \cdot (w' - w) - |OO''| \geq (w' - w) - |OO''| = d$$

since $k \geq 1$. As a consequence, d_k remains positive, and thus the expanded R is still contained in the expanded R′. The same reasoning can be applied for all 4 boundaries of R′. $\qquad\square$

A.2   Dataset

An example image of the dataset we used in this study, along with the corresponding GT annotations, is shown in Figure 11.

Fig. 11. Example image sample from the CARLA dataset with annotations used for the experiments.

A.3   Evaluation of DNN Safety Post-Processors

By inverting Question 1, given a k value, the minimum required IoU while still covering the whole GT label and achieving collision-freeness can be derived from Equation 9:

$$\mathsf{IoU} = \frac{2}{1+k} \tag{15}$$

This means, given an example k value of 1.5, we can compute a minimum required IoU (= 0.80 in this case) to fully cover an object in every possible case the IoU is equal or larger than this value. As a consequence, this calculation enables the IoU metric to be now connected to safe detection and being used to evaluate the performance of 2D bounding box object detection algorithms appropriately.